ATLAS Note

MUON-2016-XX

Draft version 0.1

Design, Construction, and Commissioning of the BME sMDT Chamber for the ATLAS Muon Spectrometer

O. Kortner[a], H. Kroha[a], F. Sforza[a], E. Takasugi[a]

[a]*Max-Planck-Institut fuer Physik, Munich*

24th May 2017

This note summarizes the design, construction and installation of the sMDT BME chambers for the BME elevator region upgrade.

Contents

1 Introduction

The Monitored Drift Tube (MDT) chambers are one of four systems in the ATLAS Muon Spectrometer (see Fig. 1). The other systems are the Cathode Strip Chambers (CSCs), Thin Gap Chambers (TGCs), and Resistive Plate Chambers (RPCs). The MDT chambers have demonstrated that they provide very precise and robust tracking over large areas of the Muon Spectrometer. The Muon Spectrometer is designed to detect charged particles at pseudo-rapidities of $|\eta| \leq 2.7$ and accurately measure their momenta. More information about the Muon Spectrometer can be found in the ATLAS Muon TDR [1].

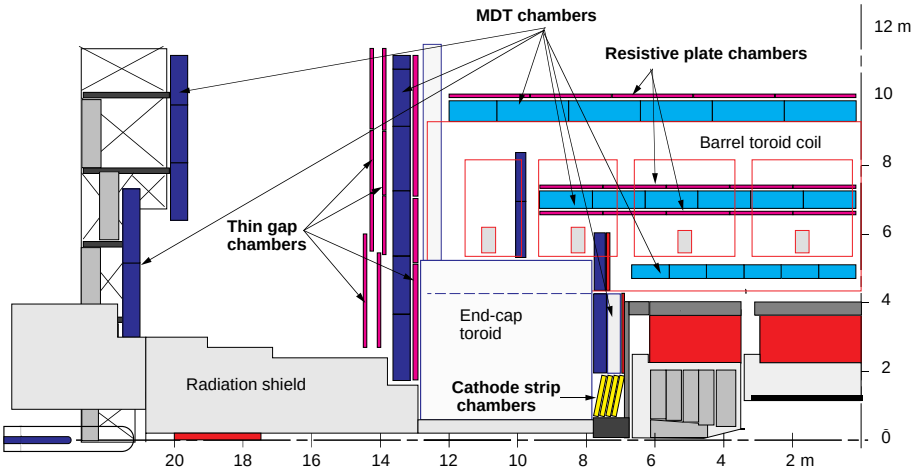

Figure 1: Quadrant view of the ATLAS Muon Spectrometer. The MDT chambers in the barrel (light blue) and in the endcap (dark blue) are in three layers. Figure from the ATLAS Muon TDR [1].

2 Monitored Drift Tube (MDT) Chambers

The MDT chambers are the main system for the ATLAS Muon Spectrometer's precision tracking system. They are precisely constructed and constantly monitored to quantify any deformations or changes in position during operation. The MDT chambers provide the primary momentum measurement in the Muon Spectrometer. They use pressurized drift tubes which are 30 mm in diameter and filled with Ar/CO_2 gas (with a 93:7 ratio), pressurized to 3 bar.

The MDT chambers are arranged into three layers in the barrel and three layers in both of the endcaps. The three layers in the barrel form coaxial cylinders around the beam axis, and the endcaps form circular disks all centered on the beam axis. The chambers in the innermost layer (both in the endcap and in the barrel) consist of eight layers of tubes, split into two equal multilayers, whereas the remaining chambers consist of six layers of tubes, also split into two equal multilayers. The chambers themselves are rectangular in the barrel region, but trapezoidal in the endcaps to create circular disks of MDT chambers. A table of the general MDT chamber parameters can be seen in Tab. 1.

A cross-section of one drift tube can be seen in Fig. 2. As a charged particle passes through the tube, the Ar/CO_2 gas is ionized. The electrons from the ionization clusters drift toward the anode wire. These drift velocities depend strongly on the radius, ranging from 10 μm/ns close to the tube wall, 26 μm/ns halfway between the wall and the wire, and 52 μm/ns close to the wire. These electrons create a sequence of pulses

Table 1: MDT chamber parameters.

Parameter	Design value
Tube diameter	30 mm
Wire diameter	50 μm
Gas mixture	Ar/CO_2 (93:7 ratio)
Gas pressure	3 bar (absolute)
Gas gain	2×10^4
Wire potential	3080 V
Average drift velocity	$\sim$ 20.7 μm/ns

which are read out by the electronics seen in Fig. 3. More details about the MDT chamber electronics can be found in [2].

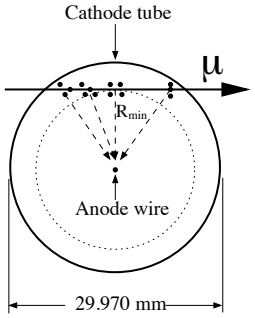

Figure 2: Cross section of a tube from an MDT chamber [2].

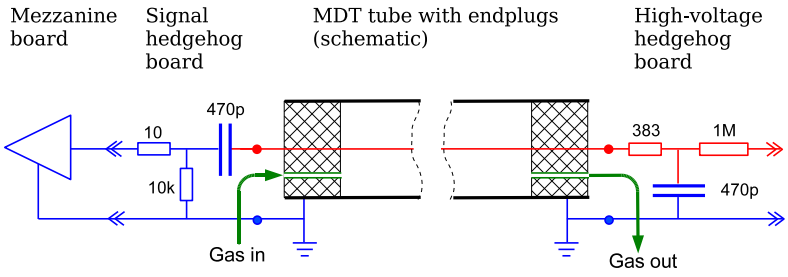

Figure 3: Schematic of a tube from an MDT chamber [2].

3 Small-Diameter Monitored Drift Tube (sMDT) Chambers

Small-diameter Monitored Drift Tube (sMDT) chambers utilize the same technology as the existing MDT chambers. However they differ in one major way: the tube diameter used is reduced by a factor of two in the sMDT chambers as opposed to the MDT chambers. This leads to a maximum drift time in the sMDT chambers which is almost one-fourth the time in a standard MDT chamber (see Fig. 4). This allows for an increase in rate capability of these new tubes of approximately one order of magnitude. Furthermore, the sMDT chambers themselves are geometrically smaller allowing them to be fitted into locations where standard MDT chambers are too large.

Table 2: MDT versus sMDT chamber parameters. The difference in HV ensures that the electric field inside the tubes, and therefore the gas gain, is identical in both types of chambers.

Parameter	MDT	sMDT
Diameter	30 mm	15 mm
Maximum drift time	700 ns	185 ns
Wire potential	3080 V	2730 V
Wire diameter	50 μm	
Gas mixture	Ar/CO_2 (93:7 ratio)	
Gas pressure	3 bar (absolute)	
Gas gain	2×10^4	
Chamber resolution	$\sim$ 40 μm	

The BME sMDT chambers are designed to cover the gaps in the ATLAS Muon Spectrometer due to the elevator region of the ATLAS detector, illustrated in Fig. 5. They are offset from the actual gaps themselves as the elevator regions must remain clear. The BME chambers will have two positions, as the "run" position which covers the gap (for data-taking) does slightly overlap access in the elevator region. As such, a second "parking" position is designated for when access must be made to the cavern (see Fig. 6). Also crucial is that the chamber can reliably return to the same place from "parking" to the "run" position. This is done by rail supports mounted on the frame. These supports, in conjunction with the alignment system can return the chamber to an accuracy of 30 μm with respect to the ATLAS Muon Spectrometer. The diagonal lines starting at the interaction point (IP) show the coverage of the chambers in $\eta - \phi$ space even though the chambers are offset from the elevator gap. There are two BME chambers, one for the A side and one for the C side. Over 1,000 tubes are required for the construction of these sMDT chambers. Each chamber takes approximately one month to complete, after which their seals and electronics are tested.

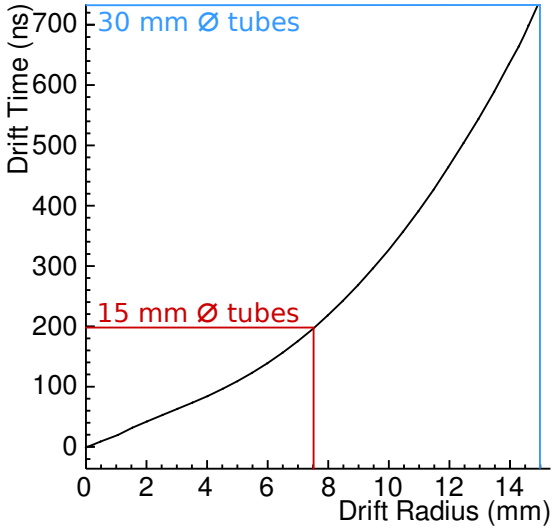

Figure 4: Maximum drift time versus tube radius. The old 30 mm tube drift time is noted in blue, whereas the new 15 mm tube drift time is noted in red.

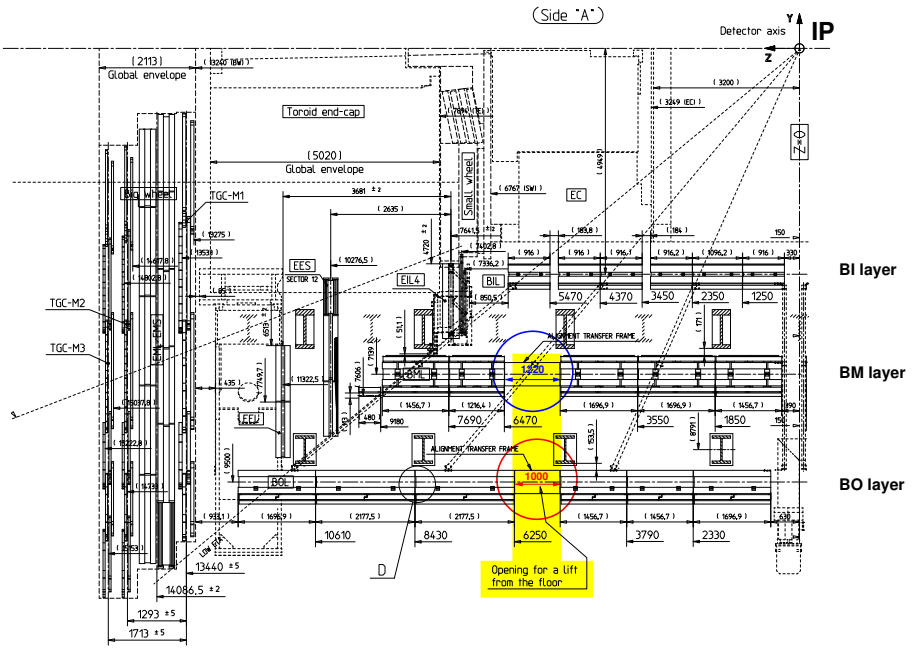

Figure 5: Quadrant view of the ATLAS Muon Spectrometer. The elevator regions are highlighted in yellow. The gaps in the Barrel Middle (BM) and Barrel Outer (BO) layers are circled in blue and red, respectively. The gap circled in blue is the region covered by the BME sMDT chambers. The red gap was covered by the BOE chambers installed in February 2013. The elevator gap is indicated by the yellow box [3].

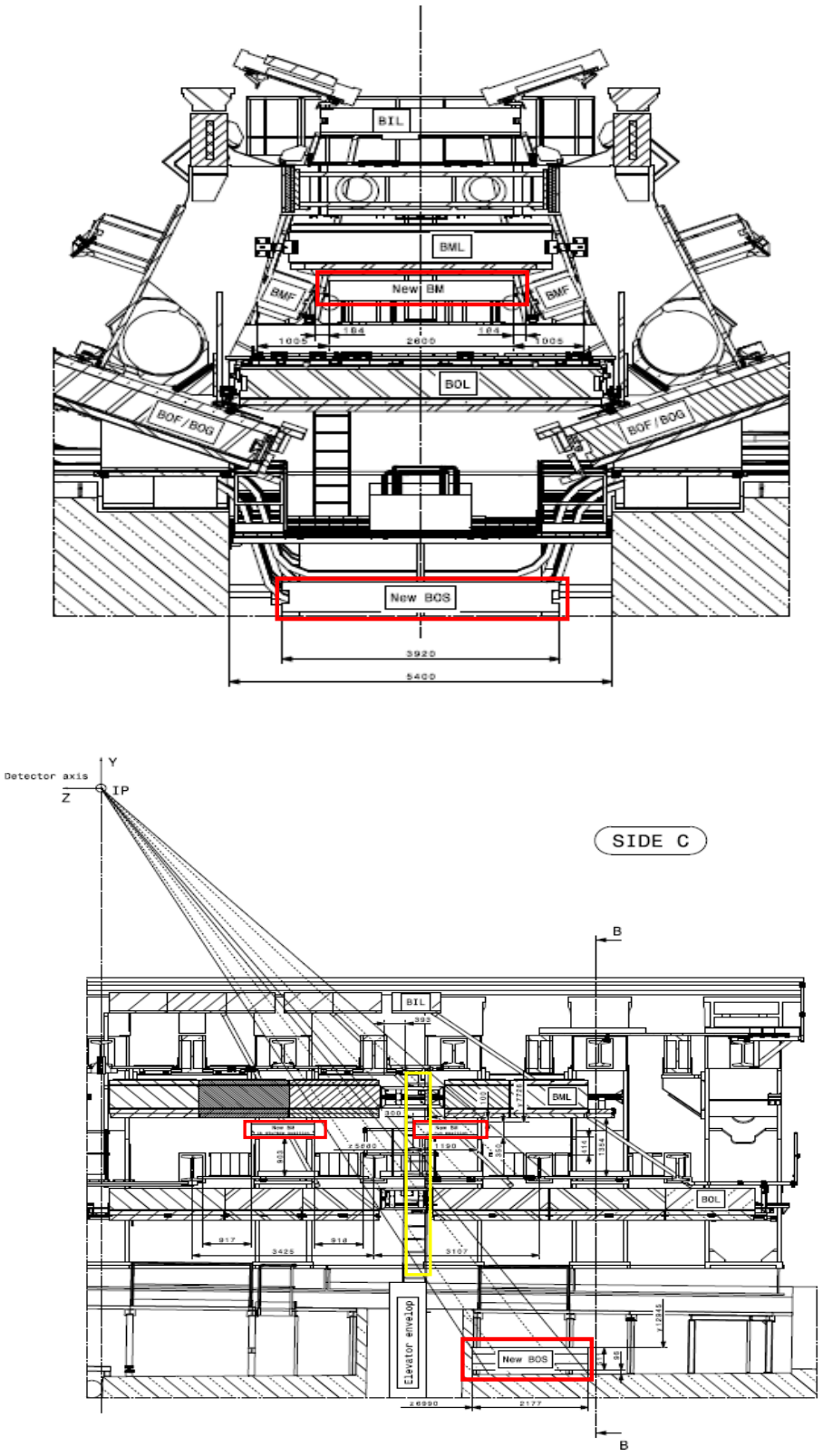

Figure 6: Location of the BME and BOE chambers. An $r-\phi$ view can be seen in the top figure, with the locations of the BME and BOE chambers highlighted in red. The upper box indicates where the BME chambers will be, and the BOE chambers are indicated by the lower box. In the lower figure is an $y-z$ slice, with the BOE chamber location boxed in red at the bottom. The two upper red boxes indicate the "parked" (left) and "run" (right) positions for the BME chambers [3].

4 sMDT BME Chamber Construction

The sMDT BME chamber construction takes place inside a clean room at MPI Munich. Each individual tube used in the sMDT chambers is 2150 mm in length with a 15 mm diameter. Endplugs on either end cap the tube. Each tube is recorded in an MySQL database[4] along with the results from every test conducted on the tubes[1].

Each new sMDT chamber consists of two multilayers of tubes. Every multilayer has four layers, each with 78 tubes. In between each multilayer is a frame which has two beams along the tube direction (also named long-beams), and three cross plates perpendicular to them: one at the center and two at the extremities of the chamber. Two additional reinforcing brackets are screwed close to the extremities of the long-beams to avoid torsion of the chamber. The middle cross plate is equipped with two adjustable screws joined to the long-beams. The screws can be used to adjust the position of the drift tubes by few tens of microns upward or downward as they will be glued on the middle cross plate in a completed chamber. This allows to compensate the gravitational sag affecting the anode wires and to achieve the maximal centrally of the wires across all the drift-tube length. The frame is supported on a 3-point kinematic mount that is used to install the chamber in the ATLAS detector and it is designed to give the minimal stress on the structure.

An in-plane alignment system is also installed on this frame. This system, called RasNiK, has four infrared LEDs on one of the external cross plates, four adjustable lens on the middle cross plate, and two CCD able to record the pattern illumined by the LEDs. This system is used to monitor deformation of the frame at the level of few microns (for more details, see [5]).

Surrounding the tube layers is the gas system, HV and RO electronics, a Faraday cage, and protective covers, similar to the MDT chambers (see Fig. 3). Furthermore, on-chamber electronics boxes were installed. On the exterior, kinematical supports as well as survey target supports were installed. A protective cover was installed over any remaining exposed surfaces. In total, the new sMDT BME chambers required 1,248 tubes.

5 sMDT Tube Construction and Testing

The tube construction starts with the crimping of one endplug into the tube. The Tungsten-Rhenium (W-Re) wire with 0.05 mm diameter is then semi-automatically threaded into the tube using air pressure (see Fig. 9). The wire is then fastened to the first endplug with a copper tubelet, fixing the wire in place on one end. The second endplug is crimped, but the wire is not fixed on this end of the tube. These endplugs not only hold the wire at the correct position (± 5 μm) and tension, but also provide an airtight seal for the tube and enable HV supply and signal readout. A cross section of a tube can be seen in Fig. 7, and an exploded view and cutaway of an endplug can be seen in Fig. 8 with the gas system and grounding system.

The wire is then tensioned to 400 g for 10 seconds. This tension is removed, and the wire is re-tensioned to 350 ± 15 g. This tension is fixed with another copper tubelet on the other end, which is crimped into place.

[1] The database can be found at: http://134.107.29.19/ for sMDT tube production (BME, BMG, and BIS productions), and http://134.107.29.19/BME_all_tubes_overview.php for BME specific tubes. These pages are only accessible from within the MPI network.

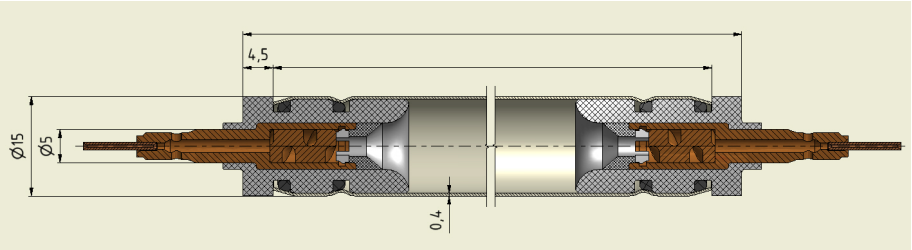

Figure 7: Cross section of one sMDT tube with dimensions of various portions noted.

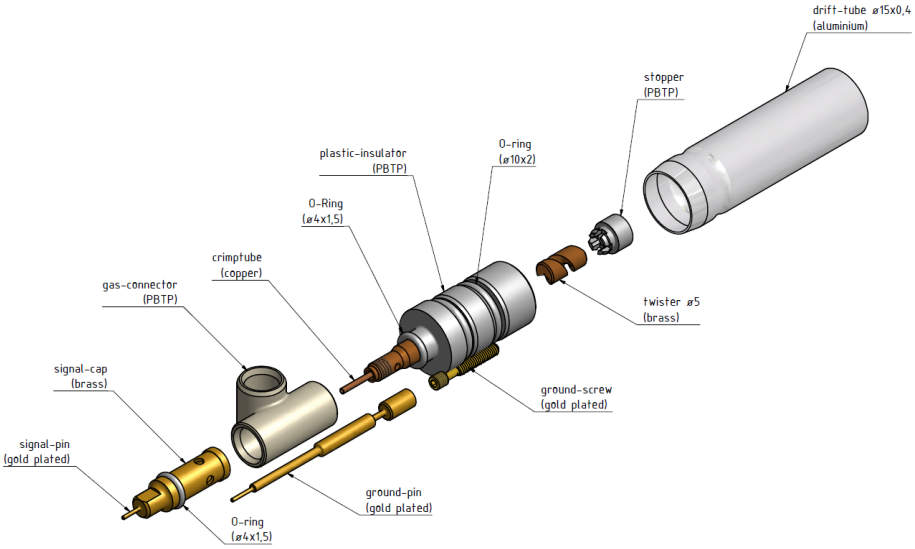

Figure 8: Exploded view of the tube endplug. Included in the lower left is the gas connection as well as signal readout as well as the grounding pin and screw for the tube.

The wire tension is checked by applying a magnetic field to the wire, and passing an alternating current across the wire, which vibrates it. By noting the vibrational amplitude of the wire, the fundamental frequency of the wire can be found, which is directly related to the tension of the wire:

$$T = \frac{\pi L^2 d^2 f^2 \rho}{g} \tag{1}$$

where T is the tension in grams, f is the frequency, d is the diameter of the wire, L is the length of the wire, and ρ is the density of the wire. Tab. 3 show the values used in the calculation. Furthermore, this measurement can be done without breaking the airtight seal on the tube endplugs and can be repeated multiple times (see Fig. 10).

Over the course of tube construction, a selection of tubes had their tension re-tested to measure any change in tension over time due to, e.g., a relaxing or stretching of the wire. This second test showed that there is a loss in tension (Fig. 11). However, it was very low at approximtaely 2% of the wire tension. The production tension was already high enough to allow for this relaxation. These results are stored in the online MySQL database.

The results of the tension test are shown in Fig. 12. The tension limits (355 ± 15 g) are shown in dotted

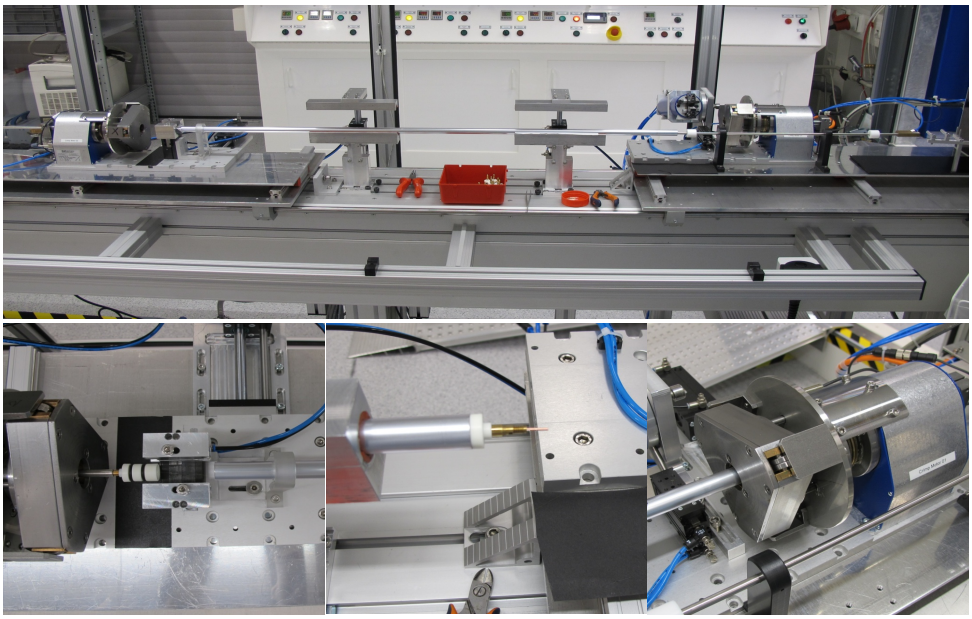

Figure 9: Wiring machine (top) with closeup of the endplug before insertion into the tube (bottom left), after insertion (bottom center), and component which affixes the endplug into the tube (bottom right).

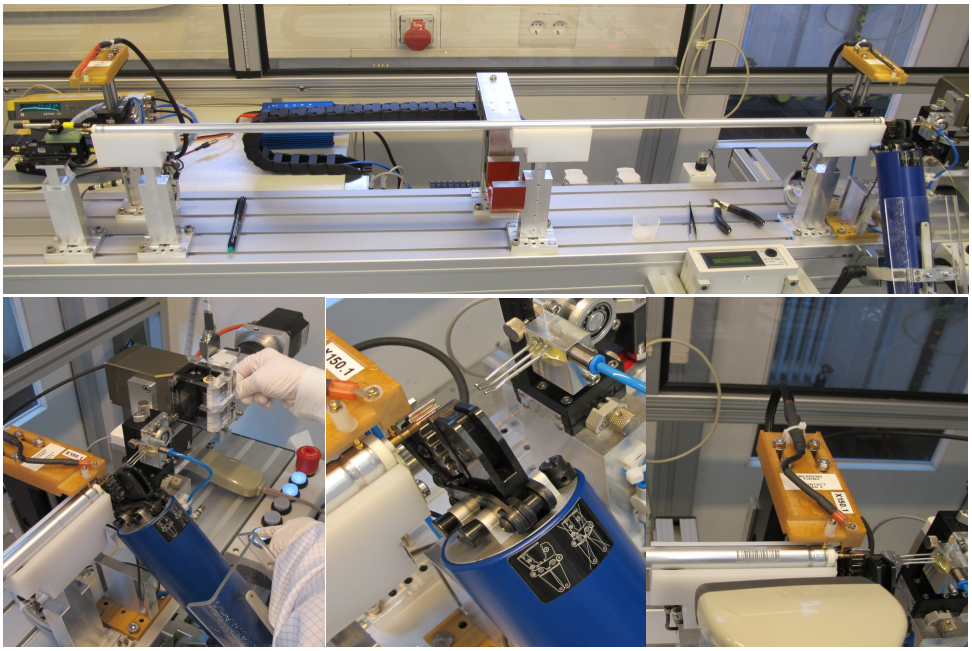

Figure 10: Wire tensioning machine (top), with a closeup of the tensioning device (bottom left), tube crimping (bottom center). The final step of entering the fundamental wire frequency and resistance into the database using the barcode associated with the tube (bottom right). The red component in the center of the top image is the magnet which, coupled with an alternating current, allows for a measurement of the wire tension without opening the tube.

Table 3: Wire parameters used in the calculation of the wire frequency using Eq. 1.

Constant	Value
L [mm]	2130
d [mm]	5×10^{-5}
ρ [g·cm^{-3}]	19.3
g [m/s^2]	9.81

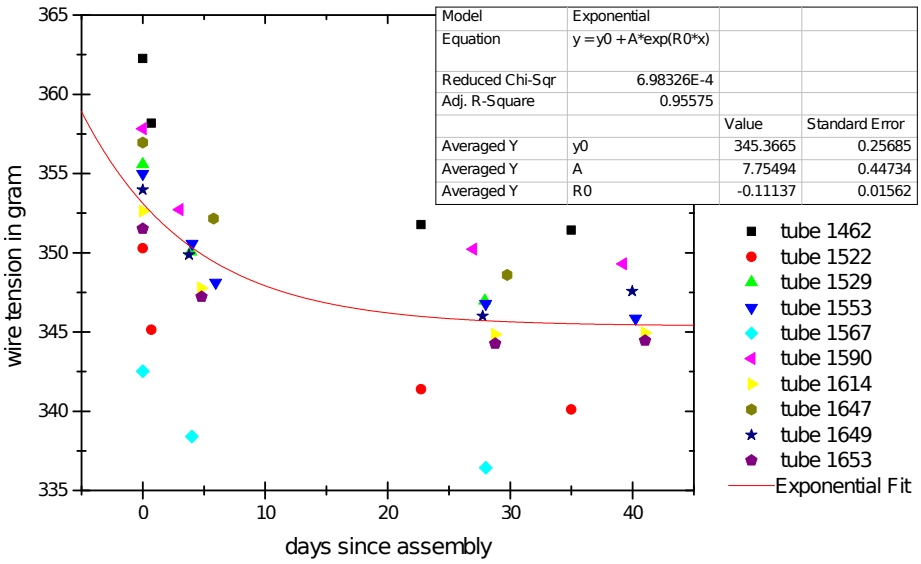

Figure 11: Loss in tension as a function of time. An exponential fit to the average wire tension loss is shown in red. The tension stabilizes after approximately one week.

red lines. All passing tubes are colored green, while the failing tubes are colored red. The majority of the tubes pass, with most of the tubes being clustered around 355 g. The majority of tubes (over 2,000 out of about 2,300, or 85.6%) pass the tension test.

Once the wire has been tensioned and measured, the gas seals are tested on the tube. The gas tightness was checked by first evacuating the drift tube and checking the volume of helium leaking in the tube from the air in the clean room (see Fig. 13). This procedure has the draw back of testing the tube under vaccum with respect to the external atmospheric pressure, instead that testing the tube at 3 bar pressure as the operating condition of the chamber. This was decided because of the tight time constraints of the chamber production and it was clear from previous studies that either end plug sealing was extremely tight or, if there were some sort of proble, the end plug would fail in a macroscopic way. The gas leakage is required to be less than 10^{-5} mbar·l/s of argon. The leak rates are also recorded on the online MySQL database.

The results of the gas leak test can be seen in Fig. 14. As before, the red dotted line shows the acceptable leak rate limit of 10^{-5} mbar·l/s. Almost all the tubes (99.7%) pass this test, confirming that the tubes can consistently be made to be airtight.

After the gas seals have been tested, the sMDT tube tested for dark current at the same location. The tubes are filled with the nominal working gas (93% Ar, 7% CO_2) at 3 bar. The voltage is then slowly raised to 3,015 V, which is above the working voltage of 2,730 V. The dark current from the tube is continuously measured, and recorded after it stabilizes, which takes approximately 4 minutes (see

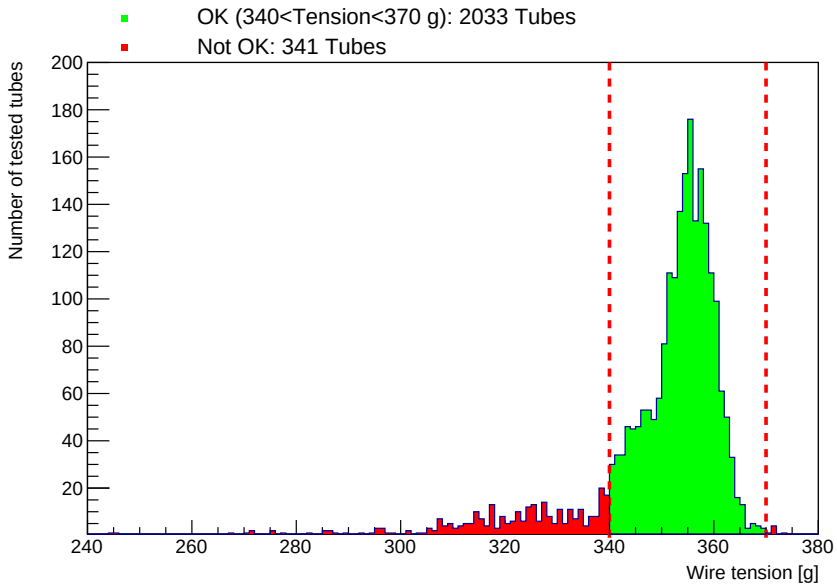

Figure 12: Tension measurements for all tested tubes. The required tension limits are shown in dotted red. The tubes which pass are in green, while the tubes which fail are in red.

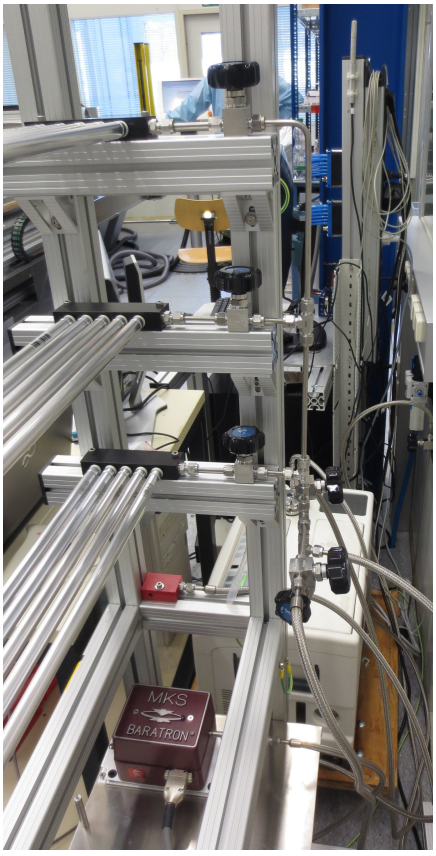

Figure 13: View of gas leak testing equipment with 15 tubes being tested. The red box at the bottom (marked "MKS BARATRON") is a barometer. The pipes on the right run between the vacuum pump, the barometer, and the tubes being tested.

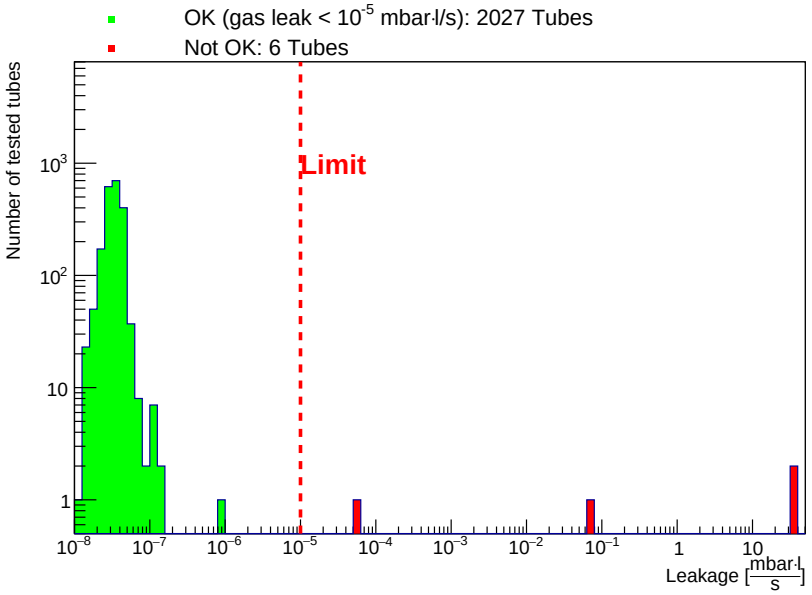

Figure 14: Measured gas leak rates for tubes. The limit (10^{-5} mbar·l/s) is shown in red. The tubes which pass are in green, while the tubes which fail are in red.

Fig. 16). The measurement device can test up to 15 tubes at a time, each with a separate HV source and current measurement device (see Fig. 15). The maximum allowed dark current is 10 nA per tube, which corresponds to 5 nA per meter of tube length. Again, all results from the current test are recorded online in the MySQL database.

The results of the HV test can be seen in Fig. 17. The limit of 10 nA is denoted by a dotted red line. The majority of tubes (95.9%) pass this test.

A chart showing the production losses can be seen in Fig. 18. The relative losses are enumerated in Tab. 4 and shown in Fig. 19. A large number of tubes pass all tests, with the main loss being due to inadequate tensioning (12.78%). The second largest loss is due to “Missing measurement”, were one of the measurements for a tube is missing. This is largely due to the fact that 1,944 tubes, or the required 1,248 tubes plus a more than adequate number of spares (over 50%) was available for chamber construction. However, the expertise gained was utilized in the BMG and BIL sMDT chamber projects.

Figure 15: HV testing apparatus. This setup can test up to 15 tubes simultaneously. On the bottom right is the HV source connected to each chamber with individual current measurements for each tube. The right hand side is seen in Fig. 13. The pipes are also connected to a gas bottle to bring the tubes up to 3 bar pressure (absolute) for the testing of the dark current. A sample plot showing the voltage and current on five of the tubes can be seen in Fig. 16.

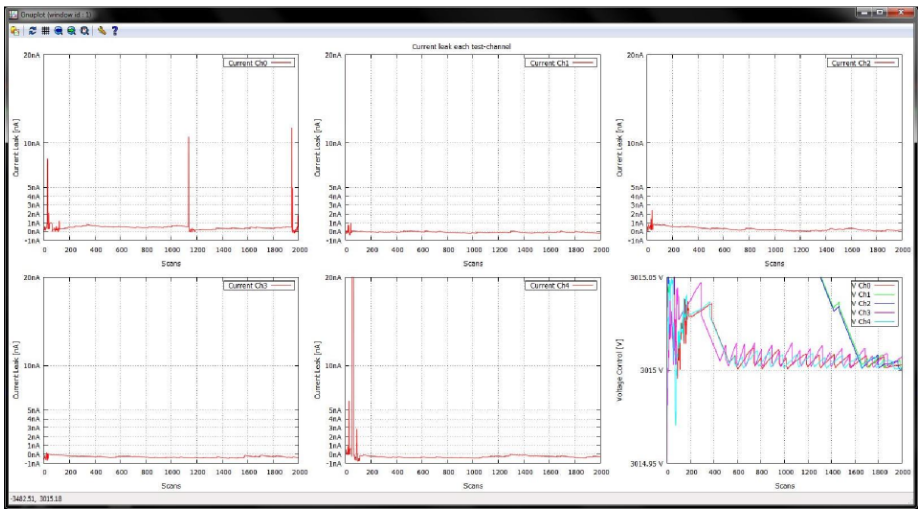

Figure 16: A sample readout of the current measurement for five tubes under test. The current and voltage stabilizes after approximately 4 minutes. The lower right shows the voltage in all five tubes over time. The remaining five plots show the measured dark current in each of the five tubes, sequencially from left to right, top to bottom.

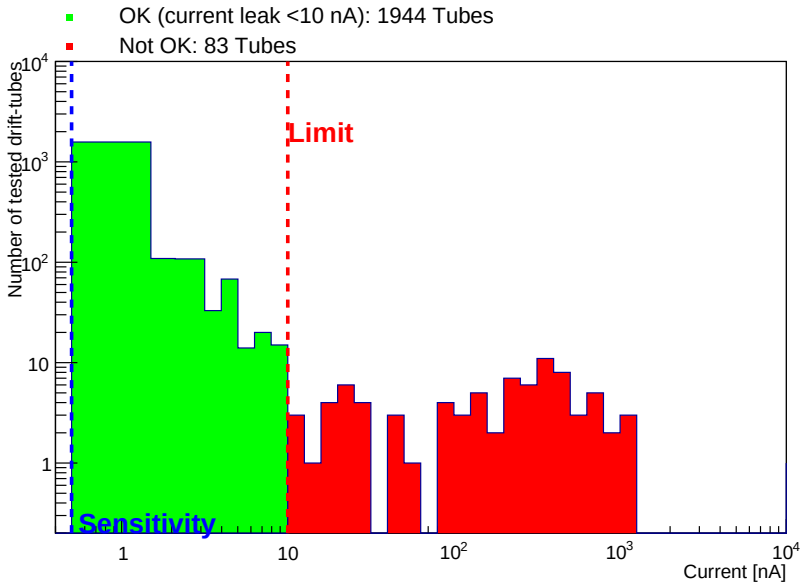

Figure 17: Measured dark current for tubes. The limit (10 nA) is shown in red. The tubes which pass are in green, while the tubes which fail are in red.

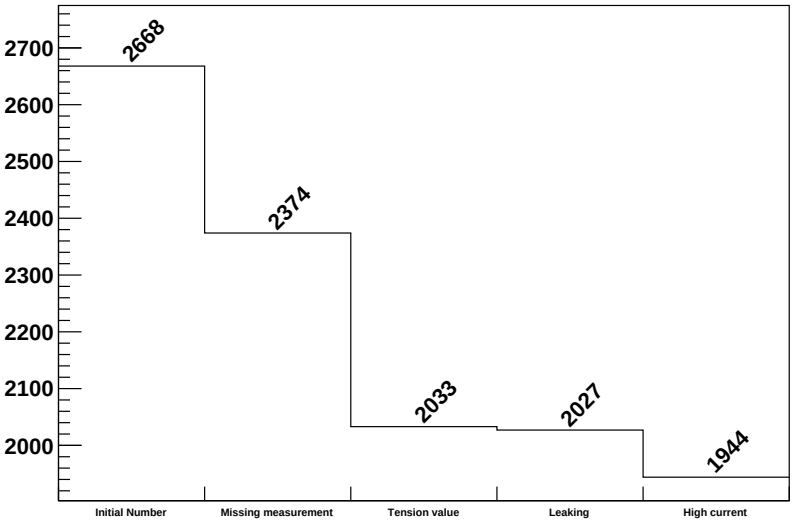

Figure 18: Number of tubes which remain after each test.

Table 4: Tube production loss percentages.

2668 Tubes	Total number
72.8636%	OK
3.11094%	High current
0.224888%	Leaking
12.7811%	Tension value
11.0195%	Missing measurement

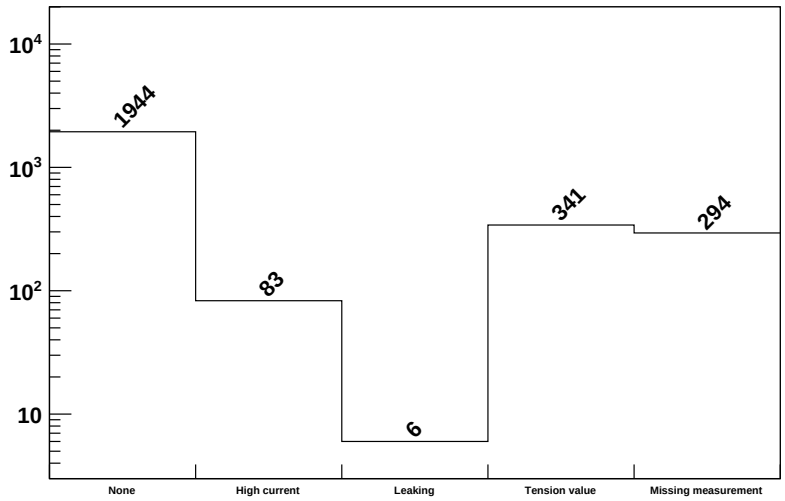

Figure 19: Tube production loss by category.

6 Chamber Construction

Once enough tubes for a chamber are produced, they are used to construct an sMDT chamber. Alignment combs are used to ensure that the tubes, and more importantly the wires inside the tubes, are positioned in the proper place. This is crucial because the wires give the position readout of hits when a charged particle, e.g., a muon, passes through the tubes in a chamber. This is done by fixing the endplugs as closely as possible to a predetermined grid pattern. For each layer in the comb, there is a bottom half and top half which come together to encase and hold the tube endplugs in place. Because of the concentricity of the wire-and-endplug assembly, precise location of the endplug leads to precise positioning of the wires within the tube. A schematic of the combs in particular can be seen in Fig. 20.

First, a layer of tubes is placed into the appropriate slots in the combs. As each tube is installed, their number, the chamber they are installed in, and their position inside that chamber is recorded in the MySQL database. Grounding pins are also inserted into the combs. After the first layer is in place, epoxy is laid down to prepare for the next layer of tubes. A weight is used to keep the tubes from shifting as the epoxy is left to set. This process is repeated until the first multilayer (four layers' worth of tubes) is installed. This process takes approximately two days.

Once the first multilayer is completed and set, it is moved off the table and a second multilayer is started. The tubes are laid down in the same manner as before until the second multilayer is also completed. Once the second multilayer is completed and set, a frame is set on top of the multilayer. A schematic of the spacer and alignment frame can be seen in Fig. 21. This must be properly aligned so that the RasNiK system can accurately measure any deformations on the chamber. Furthermore, this RasNiK system is used to make sure that the BME chamber returns to the proper "run" position with 30 μm with respect to the ATLAS Muon Spectrometer. Once the frame and alignment system is properly placed and glued, it is allowed to set.

Once the frame is in place, the first multilayer is brought on top of the frame and glued into place. Once the epoxy has set, the combs are removed and the chamber is ready for testing. A schematic for the chambers can be seen in Figs. 23 and 24.

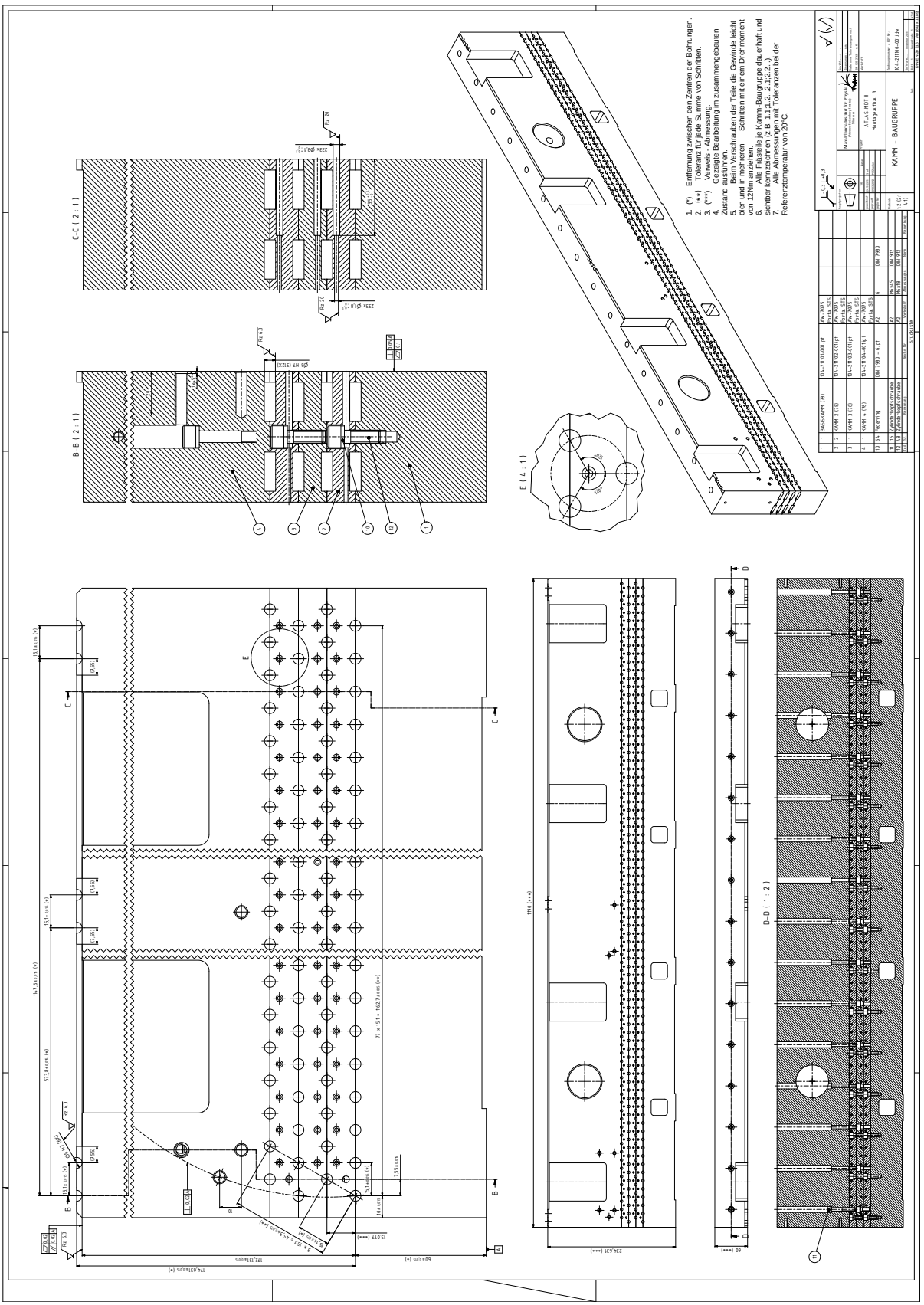

Figure 20: Schematic of the alignment combs.

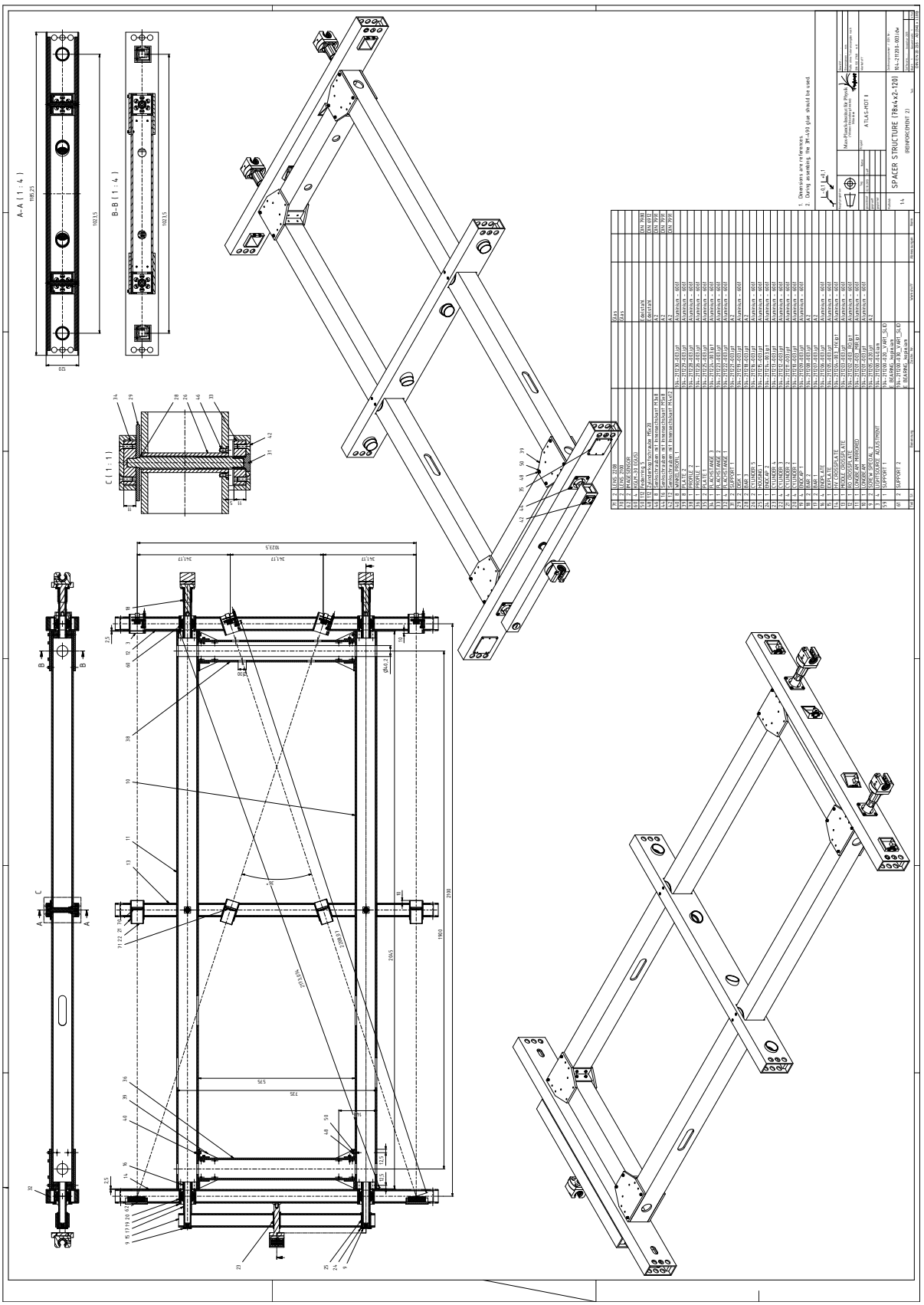

Figure 21: Schematic of the spacer and alignment frame.

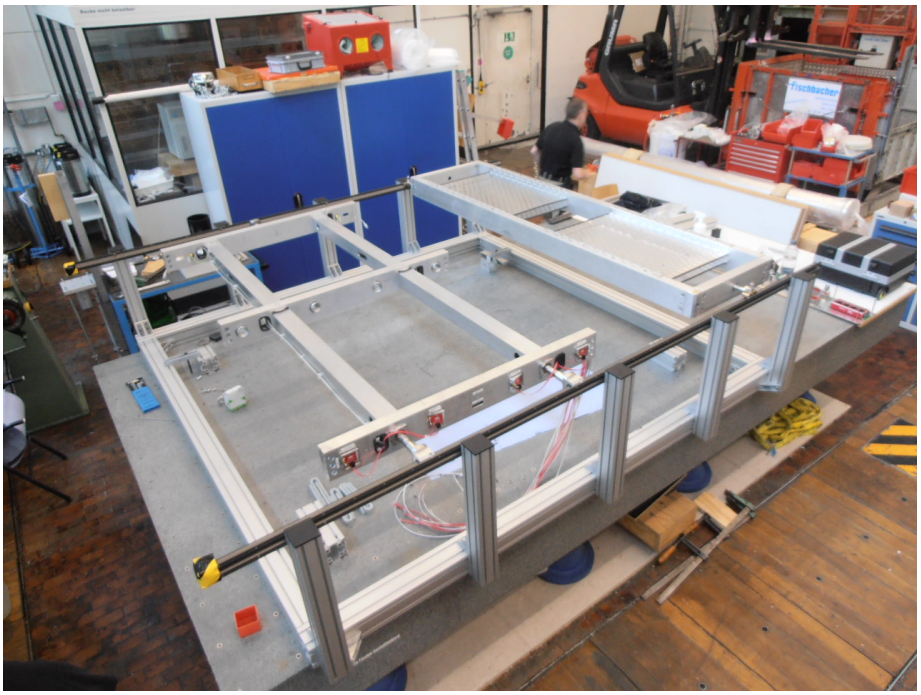

Figure 22: Image of the spacer and alignment frame.

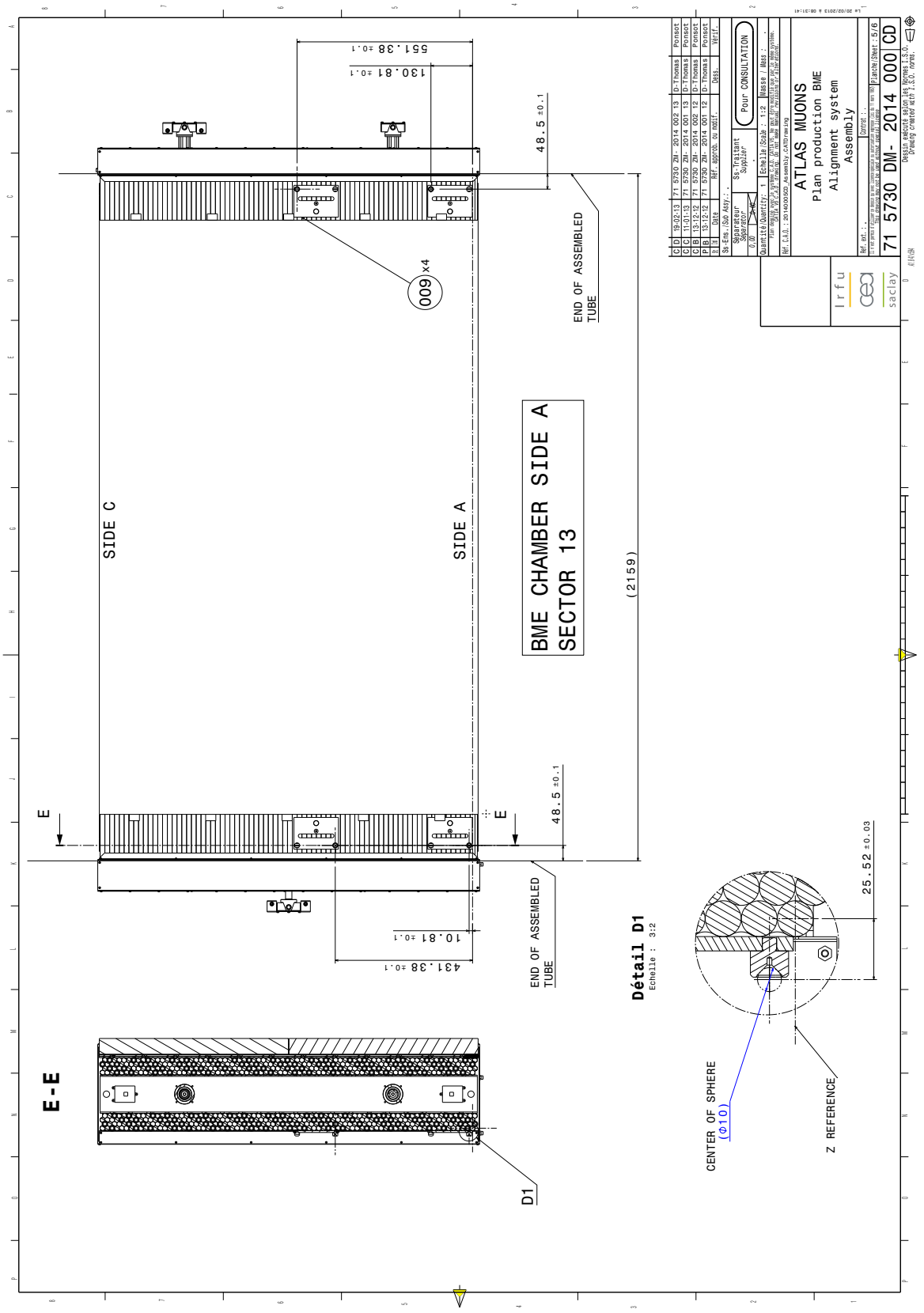

Figure 23: Complete schematic of the A side BME chamber.

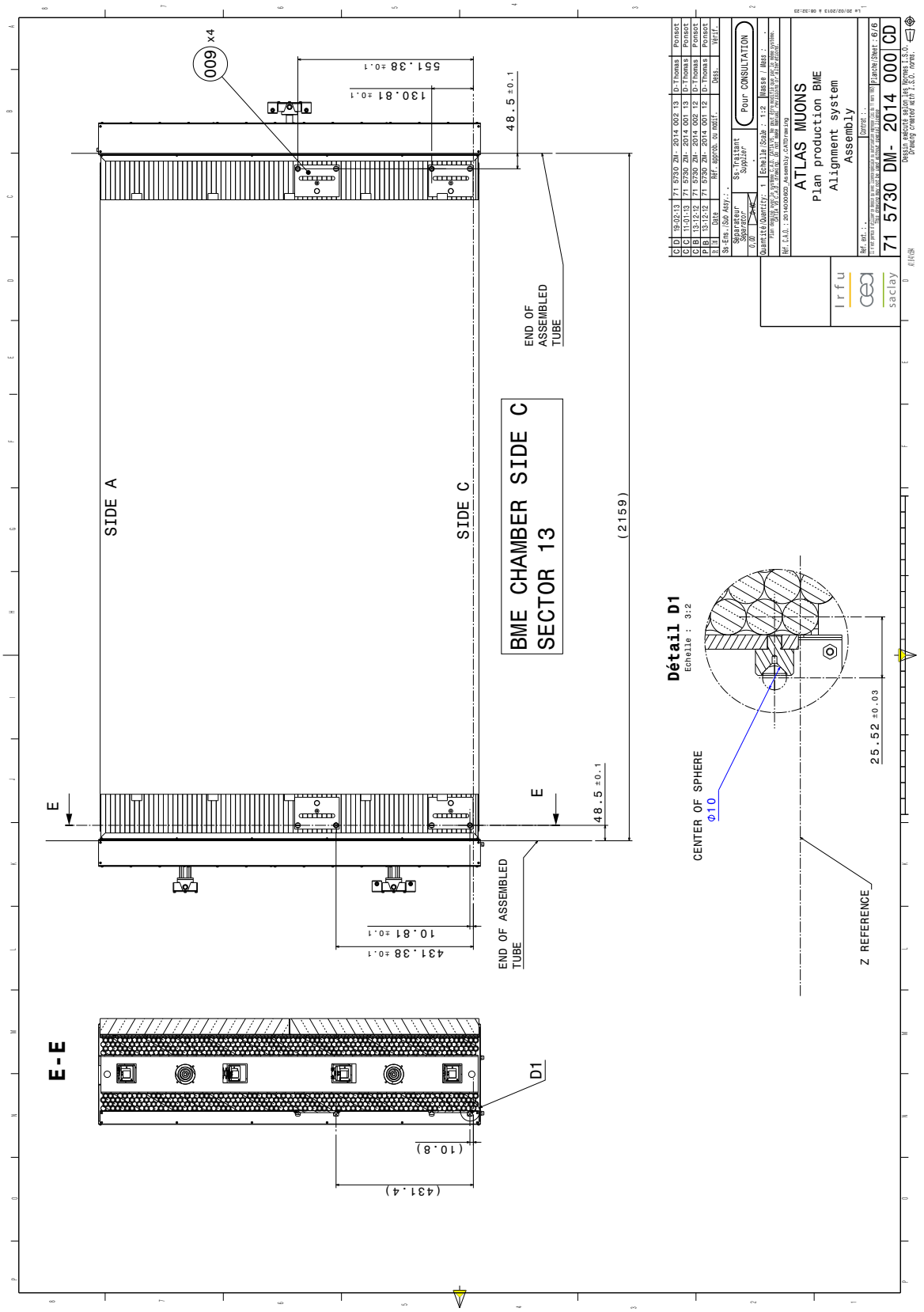

Figure 24: Complete schematic of the C side BME chamber.

7 sMDT BME Chamber Testing

7.1 Wire Position Measurement and Fitting

The concentricity between the wire and the tube endplug allows for a measurement of the wire position by measuring the position of the endplug for each tube (see Fig. 25). This is then fit to the ideal grid positions of the wires. The measurement is done on both sides of the chamber (the RO, or "South", and HV, or "North", sides, so called for the orientation of the chamber during testing). Each side is fit separately, then a combined fit is done. The results of these fits can be seen in Tab. 5 and the residuals can be seen in Tab. 27.

The fitted chamber parameters can be seen in Tab. 5, with a graphical explanation of the chambers in Fig. 26. Every chamber constructed is within nominal values. The RMS and σ of the z- and y-residuals of the fitted distributions are shown in Tab. 27. Overall, the RMS and σ of these decrease as more chambers were constructed.

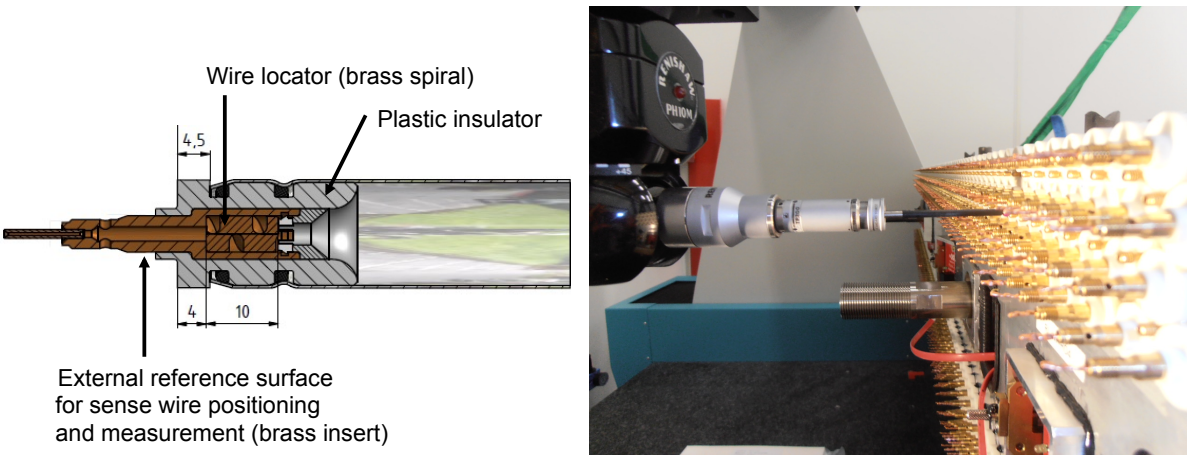

Figure 25: Cutaway of tube endplug (left), and wire measurement using endplugs (right).

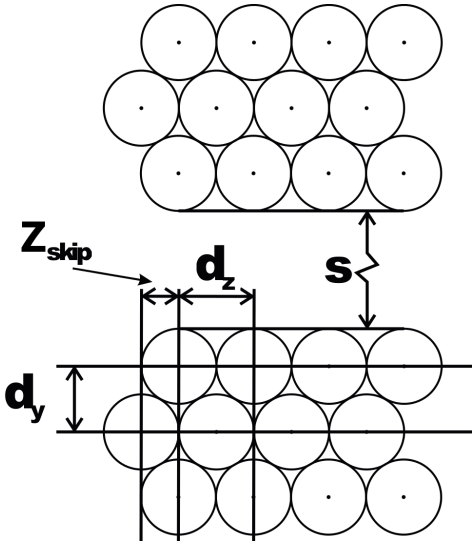

Figure 26: Graphical desciption of the various fit parameters in Tab. 5.

Grid parameters [mm]	BME-A	BME-C2
d_z	15.09923 ± 0.00001	15.09907 ± 0.00001
d_y	13.09062 ± 0.00010	13.09112 ± 0.00010
z_{skip}	−7.55186 ± 0.00023	−7.54861 ± 0.00023
s (Δz^{ML})	0.01860 ± 0.00023	0.00110 ± 0.00023
y^{ML}(North)	135.35655 ± 0.00043	135.37440 ± 0.00044
y^{ML}(South)	135.26665 ± 0.00044	135.28142 ± 0.00041
Residuals [mm]	**BME-A**	**BME-C2**
z σ Gauss fit	0.0097	0.0093
z RMS	0.0133	0.0119
y σ Gauss fit	0.0116	0.0122
y RMS	0.0163	0.0172

Table 5: Fitted wire positions. The quantities are illustrated in Fig. 26. The fit with ATLAS detector constraints is in Tab. 7.

A second fit was done to the wire position measurements based on constraints in the ATLAS detector. These second fit results are in the Appendix, in Tab. 7.

7.2 Gas, HV, and Electronics Installation

While the fits are done, the on-chamber electronics and gas systems are installed. This includes the high voltage connections to the wires, the electronics to read a signal from each tube and Faraday cages to reduce noise on the electronics. The basic schematic for the readout, HV, and gas system is similar to an MDT tube (see Fig. 3 for a basic schematic). For more details about the electronics boards, see [2].

The gas system is first installed, with inputs on the RO side and outputs on the HV side. The gas manifold

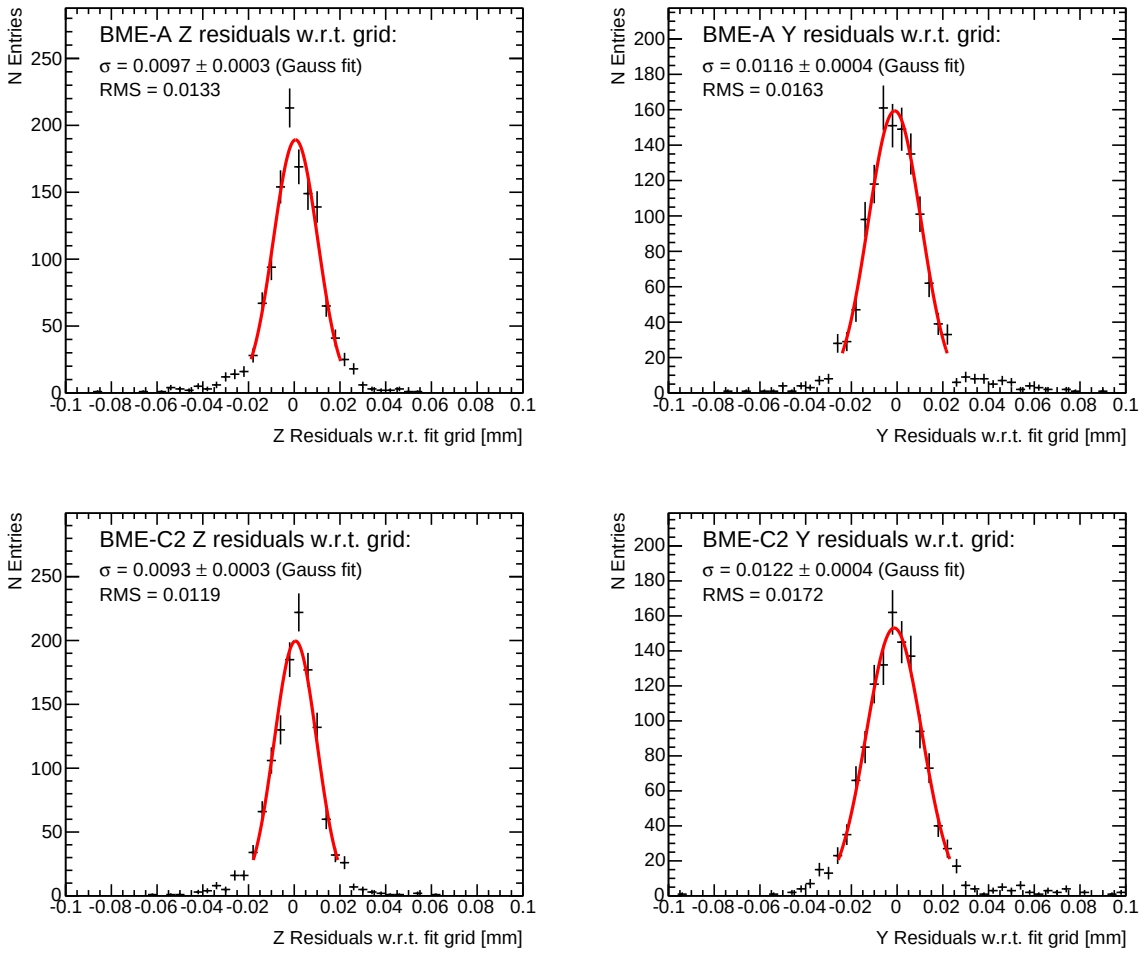

Figure 27: Residulas from the grid fit. The left are the Z residuals, and the right are the Y residuals. The top is chamber BME-A, and the bottom is BME-C2.

runs across the width of the chamber, and distributes the gas in columns of four tubes per multilayer. Each multilayer has one pair of gas bars, one for input and one for output. On the RO side, gas is filled, while on the HV side, the gas is drawn out of the tubes. These are then connected to the input and output valves installed on the RO side of the chamber. A wire-frame of the gas system can be seen in Fig. 28. A cutaway of the gas distribution into four tubes can be seen in Fig. 29. The connection of one tube to the gas system can be seen in the lower left of Fig. 8.

Two boards are installed for the readout of the tubes on the RO side. First, a signal hedgehog board, which connects directly to the tubes, is installed. These boards read the signals from up to 24 tubes. Depending on the chamber, there are locations where these hedgehog boards are not installed. These correspond to the cutouts in the tubes for the ATLAS alignment system.

On top of the hedgehog board is an aluminum plate to reduce the noise seen from the chamber. A mezzanine board is installed above this, and connected directly to the hedgehog boards. These can read out the same number of tubes (24) as the hedgehog boards underneath. There are also mezzanine cards not installed which correspond to the cutouts in the chamber (see Fig. 32). These are connected to the

CSM on the top of the chamber. The CSM provides communication between the chamber and the ATLAS system, providing the triggers to the chamber and delivering data from the chamber via optical fiber.

On the opposite (HV) side, the components for high voltage distribution are installed. The HV hedgehog cards, like the readout hedgehog boards, provide high voltage for up to 24 tubes. These are connected together via jumpers at five points: one for each of the four layers plus an additional for the ground. One card has an additional connection to the high voltage distribution box mounted on top of the chamber. The voltage distribution box takes two high voltage inputs, one for each multilayer, and distributes them, with one output cable per layer in the chamber and one last cable for ground.

Throughout the chamber, 14 temperature sensors are installed to ensure the chambers are at nominal temperature. These are connected to the MDT-DCS board on top of the chamber. This MDT-DCS board also takes input from the CSM (and thus from the mezzanine cards), providing parameters to the CSM and mezzanine cards for operation. The MDT-DCS board also provides for status and error monitoring of the CSM and mezzanine cards. Finally, Faraday cages are installed around the HV and RO electronics, and the boards on top of the chamber (CSM, DCS and HV distribution board) are also covered. A schematic of the Faraday cages can be seen in Fig. 30.

The completed chamber can be seen in Figs. 31–33. The physical parameters of the completed chambers can be seen in Tabs. 6. The chamber is then run though the final set of tests.

Figure 28: A wire-frame view of the gas system on the BMG chambers. Inset are closeups of the distribution of the gas over a vertical column of four tubes on the RO side. A similar setup is on the HV is used to consolidate the gas outputs in each multilayer.

Figure 29: A side-view cutaway of the distribution of the gas over a vertical column of four tubes.

Figure 30: A schematic of the Faraday cages which cover the RO and HV sides of the chamber. The bottom left shows the cages as seen from the RO side, the lower right as seen from the HV side. The top row show various additional views of the Faraday cages.

Figure 31: Chamber seen from HV side (right) and RO side (left) with gas and HV system installed.

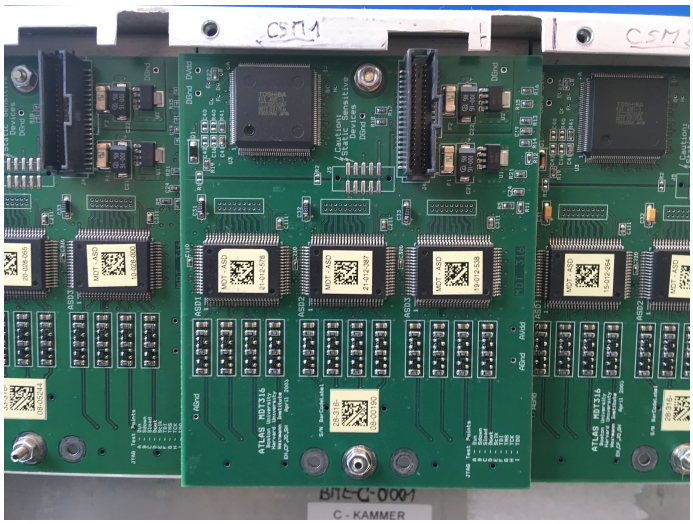

Figure 32: Chamber with readout system installed. Note: the two gaps correspond to the cutouts required for the ATLAS alignment system. In the center are the four valves, two for gas in (left side of the chamber) and two for gas out (right side of the chamber).

Figure 33: Completed chamber with Faraday cages seen from HV side (left) and RO side (right).

Table 6: Physical chamber parameters for BME chambers.

Type	BME-A	BME-C
Number of chambers	1	1
Radial distance from beam (mm)	7606	7606
Chamber width in z (mm)	1185	1185
Tubes width in z (mm)	1094.7	913.5
Chamber length in x (mm)	2325	2325
Aluminum tube length (mm)	2150	2150
Assembled tube length (mm)	2159	2159
Tube layers	2×4	2×4
Tubes/layer	78	78
Tubes/chamber	624	624
Spacer height (mm)	135.4	135.4
Tubes height (mm)	229	229
Chamber height (mm)	315	315
Gas volume/chamber (l)	212	212
Chamber weight (kg)	145	145
Mezz. cards (24 ch.)/chamber	26	26
Mezz. cards/CSM 2/1 (LH RO Side)	12	14
Mezz. cards/CSM 1/2 (RH RO Side)	14	12
Temperature sensors/chamber	16	16
In-plane systems/chamber	4	4
Survey targets	4	4

8 Conclusions

Testing conducted at MPI showed that tubes could be consistently constructed to within acceptable specifications: the tubes were gas-tight and sealed properly; the tubes had the proper tension on the wires; the wires did not loosen over time to unacceptable levels; and the tubes did not draw excessive current when brought to (and even above) their operating voltage. In the end, almost 73% of the constructed tubes pass all tests (See Tab. 4). Furthermore, this allows for spare tubes (over 50% of the required number) should any tubes become damaged.

The chambers were constructed using these tubes, and once completed, were themselves tested. In particular, the chambers were tested for their gas tightness, noise, and response to cosmic rays.

The chambers were therefore installed in the ATLAS Muon Spectrometer. The expertise gained in the construction of these chambers is being applied to the BMG and BIS7/8 projects.

Appendix

A Additional Chamber Fits

Grid parameters [mm]	BME-A	BME-C2
d_z	15.09923 ± 0.00001	15.09940 ± 0.00001
d_y	13.08872 ± 0.00009	13.08986 ± 0.00009
z_{skip}	−7.54391 ± 0.00020	−7.54026 ± 0.00020
y^{ML}	135.31410 ± 0.00037	135.32960 ± 0.00037
Residuals [mm]	**BME-A**	**BME-C2**
z σ Gauss fit	0.0158	0.0140
z RMS	0.0196	0.0156
y σ Gauss fit	0.0356	0.0320
y RMS	0.0316	0.0294

Table 7: Fitted wire positions done with ATLAS detector constraints. The quantities are illustrated in Fig. 26. The general fit is in Tab. 5

References

[1] *ATLAS muon spectrometer: Technical Design Report*, Technical Design Report ATLAS, CERN, 1997, URL: http://cds.cern.ch/record/331068.

[2] Y. Arai et al., *ATLAS Muon Drift Tube Electronics*, Journal of Instrumentation **3** (2008) P09001, URL: http://stacks.iop.org/1748-0221/3/i=09/a=P09001.

[3] G Aielli et al., 'Proposal for the Upgrade of the Elevator Regions in the ATLAS Barrel Muon Spectrometer', tech. rep. ATL-COM-MUON-2013-032, CERN, 2013, URL: https://cds.cern.ch/record/1635922.

[4] Oracle Corporation, *MySQL 5.5 Reference Manual*, URL: https://downloads.mysql.com/docs/refman-5.5-en.a4.pdf.

[5] H. Van Der Graaf et al., 'RasNiK, an Alignment System for the ATLAS MDT Barrel Muon Chambers: Technical System Description; Revised Version 2.0', tech. rep., NIKHEF, 2000, URL: http://cds.cern.ch/record/1073160.

[6] B. Bittner et al., *Development of Muon Drift-Tube Detectors for High-Luminosity Upgrades of the Large Hadron Collider*, Nucl. Instrum. Meth. **A617** (2010) 169, arXiv: 1603.09504 [physics.ins-det].

[7] H. Kroha et al., *Construction and test of a full prototype drift-tube chamber for the upgrade of the ATLAS muon spectrometer at high LHC luminosities*, Nucl. Instrum. Meth. **A718** (2013) 427.

[8] G Aielli et al., 'Proposal for the Upgrade of the Elevator Regions in the ATLAS Barrel Muon Spectrometer', tech. rep. ATL-MUON-INT-2014-001, CERN, 2014, URL: https://cds.cern.ch/record/1642793.

[9] C. Ferretti and H. Kroha, *Upgrades of the ATLAS Muon Spectrometer with sMDT Chambers*, Nucl. Instrum. Meth. **A824** (2016) 538, arXiv: 1603.09544 [physics.ins-det].

[10] H. Kroha et al., *Construction and Test of New Precision Drift-Tube Chambers for the ATLAS Muon Spectrometer*, Nucl. Instrum. Meth. **A845** (2017) 244, arXiv: 1603.08760 [physics.ins-det].

[11] H. Kroha, 'Proposal for the Improvement of the ATLAS Muon Spectrometer Momentum Resolution in Barrel Sectors 12 and 14', tech. rep. ATL-MUON-INT-2015-001, CERN, 2015, URL: https://cds.cern.ch/record/1984472.

[12] G. Aielli et al., 'The ATLAS BIS78 Project', tech. rep. ATL-COM-MUON-2016-018, CERN, 2015, URL: https://cds.cern.ch/record/2156994.

[13] M. Deile et al., *Resolution and Efficiency of the ATLAS Muon Drift-Tube Chambers at High Background Rates*, Nucl. Instrum. Meth. **A535** (2004) 212, arXiv: 1603.09572 [physics.ins-det].

[14] S. Horvat et al., *Operation of the ATLAS muon drift-tube chambers at high background rates and in magnetic fields*, IEEE Transactions on Nuclear Science **53** (2006) 562, ISSN: 0018-9499.

[15] B. Bittner, H. Kroha and O. Kortner, 'Development and Characterisation of New High-Rate Muon Drift Tube Detectors', Presented 30 Jul 2012, PhD thesis: Munich, Tech. U., 2012, URL: https://cds.cern.ch/record/1479585.

[16] P. Schwegler and H. Kroha, 'High-Rate Performance of Muon Drift Tube Detectors', Presented 14 07 2014, PhD thesis: Munich, Tech. U., 2014, URL: https://cds.cern.ch/record/1746370.

[17] B. Bittner et al., *Performance of drift-tube detectors at high counting rates for high-luminosity LHC upgrades*, Nucl. Instrum. Meth. **A732** (2013) 250, arXiv: 1603.09508 [physics.ins-det].

[18] O. Kortner et al., *Precision muon tracking detectors and read-out electronics for operation at very high background rates at future colliders*, Nucl. Instrum. Meth. **A824** (2016) 556.

[19] P. Schwegler et al., 'Optimization of the front-end electronics of Drift Tube chambers for high-rate operation', *2014 IEEE Nuclear Science Symposium and Medical Imaging Conference (NSS/MIC)*, 2014 1.

[20] S. Nowak et al., 'Optimisation of the Read-out Electronics of Muon Drift-Tube Chambers for Very High Background Rates at HL-LHC and Future Colliders', tech. rep., 2016 7581815, arXiv: 1603.08841 [physics.ins-det], URL: https://inspirehep.net/record/1436364/files/arXiv:1603.08841.pdf.

[21] J Christiansen, 'HPTDC High Performance Time to Digital Converter', tech. rep., Version 2.2 for HPTDC version 1.3: CERN, 2004, URL: https://cds.cern.ch/record/1067476.

[22] S. Nowak et al., *Construction and test of high precision drift-tube (sMDT) chambers for the ATLAS muon spectrometer*, PoS **TIPP2014** (2014) 302, arXiv: 1407.0285 [physics.ins-det].